Electric Vehicle Battery Thermal and Cabin Climate Management Based on Model Predictive Control

Yuanzhi Liu
Department of Mechanical Engineering,
The University of Texas at Dallas,
Richardson, TX 75080
e-mail: yuanzhi.liu@utdallas.edu

Jie Zhang[1]
Department of Mechanical Engineering,
The University of Texas at Dallas,
Richardson, TX, 75080
e-mail: jiezhang@utdallas.edu

Energy management plays a critical role in electric vehicle (EV) operations. To improve EV energy efficiency, this paper proposes an effective model predictive control (MPC)-based energy management strategy to simultaneously control the battery thermal management system (BTMS) and the cabin air conditioning (AC) system. We aim to improve the overall energy efficiency and battery cycle-life, while retaining soft constraints from both BTMS and AC systems. The MPC-based strategy is implemented by optimizing the battery operations and discharging schedules to avoid a peak load and by directly utilizing the regenerative power instead of recharging the battery. Compared with the benchmark system without any control coordination between BTMS and AC, the proposed MPC-based energy management has shown a 4.3% reduction in the recharging energy and a 6.5% improvement for the overall energy consumption. Overall, the MPC-based energy management is a promising solution to enhance the battery efficiency for EVs.
[DOI: 10.1115/1.4048816]

Keywords: energy management system, battery thermal management system, cabin air conditioning system, model predictive control

1 Introduction

There is a growing demand in vehicle electrification due to the widespread environmental consciousness and stringent emission regulations [1]. Lithium-ion battery (LIB) has been widely accepted as one of the most promising energy storage and electrification solutions due to its excellent properties such as high energy density and long cycle life. However, extensive investigations have pointed out that the performance and safety of lithium battery are highly affected by the temperature variations and extreme temperatures in particular. In addition, there also exist several drawbacks considering the maximum-rate discharging and cycle-life for battery system under intense-driving or peak-load conditions simultaneously [2]. Therefore, an effective energy management strategy that integrates battery thermal control is crucial to address safety concerns and to enhance energy efficiency.

1.1 Review of Air-Based Battery Thermal Management System and Control Strategy. Battery thermal management system (BTMS) plays a critical role in maintaining a reasonable temperature range (20 °C to 45 °C) for LIB due to its intrinsic chemistry properties. State-of-the-art technologies employ air, fluid, phase-changing material, and heat pipe as the transfer mediums to dissipate the over-burden waste heat [3]. There has been an increasing popularity towards integrating the phase-changing material and heat pipe in lab tests, however, due to the complexity, only the air-based and liquid-based technologies have been successfully applied to industry. For pure air-based cooling technologies, a large number of novel ventilation structures and optimal configuration settings have been proposed and verified, such as conventional *Z*- and *U*-type parallel/tapered cooling structures with optimal cooling channel settings [4–6], the modified *J*-type structure with two control valves for control mode switching [7], the reciprocating straight-forward structure with two inlet flip door valves that are used to shift the flow inlet [8], the flat-plate and cylindrical stack structure with counterflow arrangement that can change the flow direction periodically [9], the parallel stagger-arranged configuration for cylindrical battery [10], and the cubic configurations for cylindrical battery cells with varying inlet and outlet locations [11].

It is noticed that the research foci tend to be shifted from conventional steady-state structure design and modification to dynamic integrated control and optimization. Based on existing configurations, extensive control strategies have been developed to constrain the maximum operation temperature. For instance, a fuzzy logic control method was develop for a straight-forward air-based cooling system [12]; an observer-based control was employed to control the air flow direction for a reciprocating structure [13]; a hysteresis control method was utilized for a similar reciprocating flow modification [14]; and a dynamic programming together with a proportional integral-derivative control strategy was investigated comparatively to determine the best control strategy [15].

Moreover, model predictive control (MPC) and its family algorithms (e.g., constrained linear MPC, and nonlinear MPC) have been employed in several studies because of the unique characteristics, i.e., MPC forecasts steps ahead to determine optimal control solutions. It is worth noting that the MPC for thermal management usually involves with the power output and energy consumption of the battery system. For instance, Tao et al. [16] employed MPC to regulate the refrigerant compressor and cooling air flowrate to keep an ideal cooling temperature for battery pack. Masoudi et al. [17] used nonlinear MPC to extend the parallel air cooling study for Toyota Prius. Amini et al. [18] presented a hierarchical two-layer MPC scheme to schedule optimal thermal trajectories for the cabin and battery cooling in hybrid electric vehicles. The aforementioned studies have revealed the effectiveness of MPC and highlighted further potential applications in battery systems. However, the majority of these studies implemented the thermal control directly on pre-designed air-cooling structures without further

[1]Corresponding author.

Contributed by the Design Automation Committee of ASME for publication in the Journal of Mechanical Design. Manuscript received May 8, 2020; final manuscript received August 4, 2020; published online November 10, 2020. Assoc. Editor: Christopher Hoyle.

optimization, and there has not been any control co-design approach reported in the literature to design a battery cooling system. Additionally, lumped battery electric-thermal-fluid models were usually adopted for simplification, in which the battery temperature was investigated only at the cell level. The temperature distribution at the battery pack level has not yet been evaluated and validated with simulations or experiments.

1.2 Battery Energy Management Strategy. It is also noticed that the battery charging/discharging with a high power output may potentially shorten the cycle-life and affect the discharge power density [1]. From the perspective of thermal control, a high power density tends to generate a large amount of heat and bring about inevitable thermal impacts to BTMS. In consequence, it is reasonable to optimize the discharging sequence of EVs by scheduling the operations of different devices based on real-time driving conditions. Apart from the driving motor and its assisted subsystems that mainly depend on actual traffic conditions, other primary systems including the cabin climate control system/air conditioning system (AC), as well as BTMS, can be operated with a flexible energy-efficient schedule that incorporates with the driving motor jointly through load shifting.

Considering regeneration effects, the discharge scheduling and optimization refer to two approaches: (i) optimize the operation sequences of different devices and subsystems to avoid a peak demand; (ii) utilize the regenerated power directly instead of recharging the battery system. There exist similar studies in the literature regarding discharging scheduling optimization for EVs [19]. However, the majority of previous studies were performed and evaluated merely in terms of energy-saving using the aforementioned schedule optimization approach [20]. Moreover, the previous studies did not consider the side effects of the recharged energy, as well as its corresponding thermal impact on the whole battery pack under dynamic driving conditions [21].

Building on state-of-the-art thermal management and operation scheduling strategies, this paper seeks to investigate the discharging scheduling and load shifting from the thermal perspective, in which the process starts with a thermal control of the optimized battery pack and AC system, and ends up with evaluations of systematic energy efficiency. The research motivation is to develop an MPC-based strategy to improve the overall energy efficiency and battery cycle-life while well retaining thermal constraints of the battery pack. The established neural network-based J-type air-based thermal control system by the same authors is inherited in this study, in which both the plant model and controller are established with data-driven models [22]. By controlling the operation mode and the mass flowrate simultaneously, the developed BTMS has been proved to be able to maintain both the maximum temperature and the uniformity within expected ranges simultaneously. Moreover, an air precooling module is added to the existing J-type BTMS with extra cooling capability to mitigate thermal impacts from severe working conditions [23].

The contributions of this paper are threefold: (i) advanced modeling: the developed vehicle energy model simulates all heavy-duty electric devices and the BTMS at the cell level; (ii) battery recharge optimization: this paper aims to minimize the battery recharged energy by utilizing the regenerated power directly via optimization; (iii) sequential control co-design: a sequential control co-design approach [24–26] is applied to BTMS design, in which the control system is established to improve the energy efficiency after optimizing plant parameters of the J-type BTMS structure in our previous study [2].

The remainder of the paper is organized as follows. An EV systematic model is established in Sec. 2, including a battery model, a fluid dynamics model, an AC model, and a driving model. The thermal control system and overall energy management strategy are presented in Sec. 3. MPC-based management results are analyzed in Sec. 4. Concluding remarks and future work are discussed in the last section.

2 Electric Vehicle System Modeling

2.1 Battery System Modeling. Building on comparative studies of EVs network topology [27], a semi-active configuration for the battery system is adopted in this paper. The battery pack is directly connected to the DC-bus, while devices like the driving motor, the air conditioning system, the cooling fan of BTMS, and other auxiliary subsystems, are connected to the DC-bus via DC/AC converters, as illustrated in Fig. 1. The battery pack is assumed to have a capacity of 36 KWh, in which 100 cells are arranged in series (375 V) and 20 series in parallel. Note that low-voltage buses, such as 12 V bus and 48 V bus, are not considered here for simplification purposes, and all their loads are equivalently transferred to the main DC-bus. The battery electric model and thermal model are established based on Refs. [28] and [7], respectively.

The thermal characteristics of the battery are represented using a lumped model, in which there are two equivalent resistances that can be estimated using the hybrid pulse power characterization method (HPPC). It is also claimed that all sensible heat is generated by the power loss due to varying resistances [29], which highly depends on the temperature, stage of charge (SoC), and operation current I, $R = \mathcal{R}(T, SoC, I)$, as given by

$$\dot{\mathcal{G}}(T, SoC, I) = I \sum_{i=1}^{2} R_i^2 / V \tag{1}$$

where $\dot{\mathcal{G}}$ and V denote the volumetric heat generation rate and the volume of the battery, respectively. As a status indicator, SoC is usually defined using the Coulomb counting in a dynamic charging and discharging process, as given by

$$SoC_{t+1} = SoC_t \pm \frac{1}{Q_c} \int_t^{t+1} I \, dt \tag{2}$$

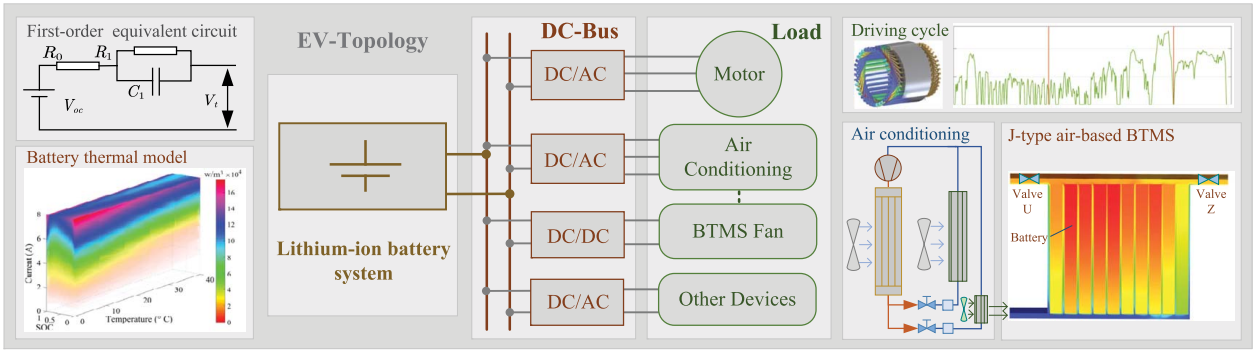

Fig. 1 The battery topology and main loads

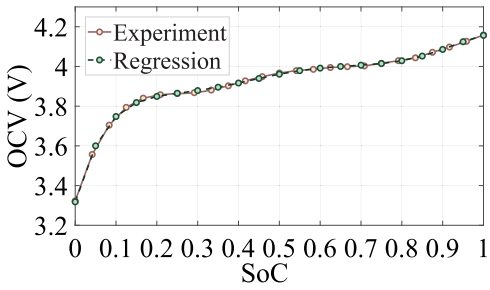

Fig. 2 The OCV-SoC correlation curve

where Q_c refers to the battery capacity. The characteristic relationship between the open-circuit voltage (OCV) and SoC is estimated using a polynomial regression, defined as

$$\begin{aligned} \mathcal{V}_{ocv} &= \mathcal{P} \cdot \mathcal{S}_{soc} \\ \mathcal{S}_{soc} &= [SoC^6 \cdots SoC^2, SoC, 1]^T \end{aligned} \tag{3}$$

The regression matrix $\mathcal{P}$ equals to [−40.2, 138.6, −186.2, 123.5, −42.4, 7.5, 3.3], as shown in Fig. 2. In consequence, the effective power output from the battery to devices is estimated using a lumped electric model, as given by

$$P_{b2dev} = (\mathcal{V}_{ocv} - I\sum_{i=0}^{N} R_i)I \tag{4}$$

On the contrary, when the discharging power is estimated by forecasting, the discharging current can be obtained via a numerical trial and error approach.

2.2 Battery Thermal-Fluid Model. Our previous study [7] has found that the *J*-type configuration with mode switching shows significant improvements for air-based BTMS in terms of maximum temperature and temperature uniformity, as shown in Fig. 1. By adjusting the opening degrees of two control valves, the battery pack is able to balance the temperature distribution between the left and the right part via switching the operation mode among the *Z*-, *U*-, and *J*-mode. Note that operation modes are predefined by the sizes of outlet manifolds, i.e., the left and right manifold sizes of *Z*-, *U*-, and *J*-mode are 4–8, 8–4, and 6–6 in millimeters, respectively, as shown in Fig. 3. Detailed investigations of the *J*-type BTMS and its corresponding control system can be found in Ref. [30].

Owing to the complexity of analytical solutions, a computational fluid dynamic (CFD) approach is adopted here, in which the channel sizes of the configuration are optimized using a surrogate-based optimization algorithm [31]. The transient flow CFD simulations are performed using ANSYS FLUENT with a k-ϵ turbulence model and a time-step of 5 s. Simulation outputs are the updated temperatures $T[.]_{k+1}$ of battery cells that are labeled as 2, 4, 7, and 9 (i.e., the middle cells of the left part and the right part of the battery pack). The inputs include the initial battery temperature $T[.]_k$, the cooling air temperature T_{air}, the mass flowrate of the approaching air $\dot{m}$, and the equivalent heat generation rate $\dot{\mathcal{G}}$, as expressed by

$$[T_2, T_4, T_7, T_9]_{(k+1)} = \mathcal{S}([T_2, T_4, T_7, T_9]_{(k)}, T_{air}, \dot{m}, \dot{\mathcal{G}}) \tag{5}$$

2.3 Dynamic Driving Model. The driving motor and its accessory system consume the largest amount of energy in EVs [32]. According to the mechanical and power analyses of a running vehicle, the equivalent traction power is estimated based on the road surface friction, gravitational potential, air friction, and acceleration, as expressed by

$$P_{drv} = \frac{v}{\eta}\left(mg\mu\,\cos\alpha + mg\sin\alpha + \frac{1}{2}\rho A_f C_d v^2 + m\frac{\mathrm{d}v}{\mathrm{d}T}\right) \tag{6}$$

The EV specification and driving conditions are summarized in Table 1. For the regenerative braking system, it is regarded as a backward of the driving mode, in which various control techniques have been developed in terms of energy harvesting efficiency and driving comfortability [33]. For simplification, it is assumed in this paper that an average of 85% (η_r) of the kinetic energy is harvested back into the power system, while the rest is dissipated irreversibly by the mechanical braking for safety concerns. The driving power is negative when regeneration occurs, as given by

$$P_{r2bus} = \frac{1}{\eta_m \eta_t \eta_r}(P_{drv_{(t+1)}} - P_{drv_t}) \tag{7}$$

2.4 Air Conditioning System Model. According to an auxiliary system impact report from the Idaho National Laboratory [35], the air conditioning system may consume up to 30% of the traction battery energy for cooling, depending on the air flow volume, and the temperature difference between the ambient environment and the cabin. The heat balance model of the electrical air conditioning system is established separately with the air conditioner model and the thermal load model, and only the temperature feature is considered in this study.

There are three major energy consuming components in the AC system, i.e., the compressor, the evaporator blower, and the condenser fan, as presented in Fig. 1. Regarding the air conditioner modeling, while a full range component level AC simulation model provides more detailed evaluations of various components with a higher accuracy, it is very challenging to manage the mathematical and computational complexity in terms of phase-changing flow, thermodynamics, and heat transfer [36]. Since this work emphasizes more on the energy perspective, the AC energy model developed in Ref. [37] is adopted. The overall power consumption of the AC system can be simplified and estimated using a ratio coefficient between the cooling capacity provided and its corresponding power consumed by the AC system, which is also referred to as the coefficient of performance (η_{cop}), given by

$$\eta_{cop} = \frac{Q_{ac}}{P_{ac}} = \mathcal{F}(T_{in}, T_{ex}, P_{lr}) \tag{8}$$

where η_{cop} is a function of the uniform internal and ambient temperatures, and the partial load ratio P_{lr}. The model is implemented

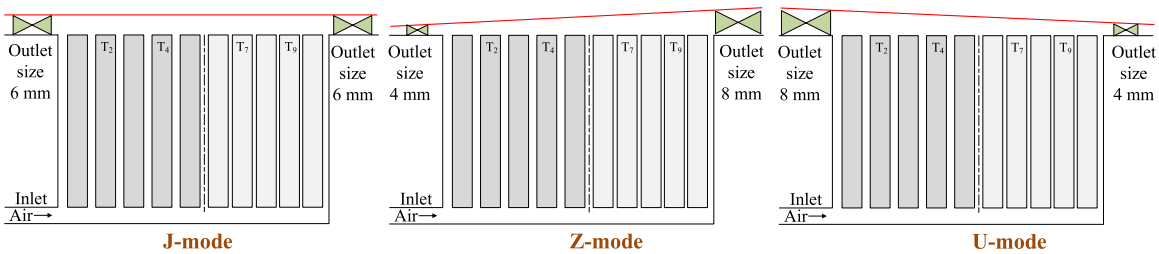

Fig. 3 The geometry configurations of the *J*-, *Z*-, *U*-mode

Table 1 Parameter specifications (data from Tesla Model 3 [34])

m	Mass	1,875 kg	α	Road gradient	0
A_f	Windward area	2.22 m^2	C_d	Air friction coeff.	0.24
g	Standard gravity	9.8 m/s^2	η	Motion efficiency	0.98
ρ	Air density	1.16 kg/m^3	μ	Rolling resistance	0.01
v	Velocity	$-m/s$	η_b	Battery coeff.	0.91
η_m	Motor coeff.	0.94	η_t	Transmission coeff.	0.97

using Gaussian process regression based on the essential data from the study conducted by Pino et al. [38].

For the thermal load model, several external and internal heat sources are generally identified and considered in the cabinet thermal model, as illustrated in Fig. 4 and tabulated in Table 2 after reasonable assumptions and simplifications. The cabin is assumed to be a trapezoidal box that has a roof panel and an interior base, surrounded by windows. Solar radiation as well as ambient air have significant impacts on internal climate via the roof panel and windows, or through window glasses. As regards the heat conduction via the roof panel or windows, it is observed that the surface temperature may probably be higher than the ambient or cabin internal temperature because of solar radiation. The heat conduction from body shell to the cabin is estimated using a heat balance method, as given by

$$Q_{cr} = \alpha IA - h_{ex}A\left(\left(\alpha I + T_{ex}h_{ex} + \frac{T_{in}}{\sum\frac{\delta}{\lambda}+\frac{1}{h_{in}}}\right)\Big/\left(h_{ex}+\frac{1}{\sum\frac{\delta}{\lambda}+\frac{1}{h_{in}}}\right) - T_{ex}\right) \tag{9}$$

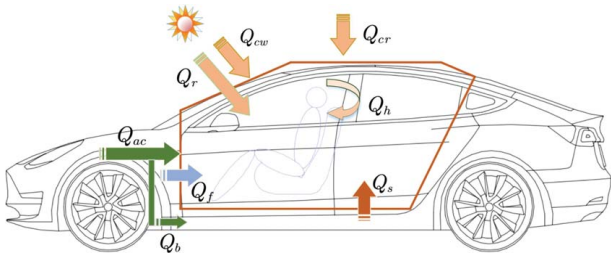

Fig. 4 The transient thermal model of a vehicle's cabin

where h_{ex} denotes the convective heat transfer coefficients between the roof panel and external ambient. h_{in} denotes the convective coefficient between the roof panel and internal cabin, I is the solar radiation, and α denotes the absorptivity. T_{in} and T_{ex} are the cabin internal air temperature and the ambient temperature, respectively. The heat conduction via windows Q_{cw} has a similar expression except the value differences of the radiation absorptivity, thickness, and thermal conductivity of glasses [39].

A previous study [40] have found that the equivalent heat transfer coefficient between the roof panel and the external ambient is highly related to the vehicle velocity, while the solar radiative thermal load through windows highly depends on both the operation time in a day and its relative whether condition. The radiation I is selected as 1,200 W/m^2 in this study. Part of the parameter settings in this model come directly from the AC simulation toolbox *coolsim* developed by the National Renewable Energy Laboratory [41] and Ref. [39]. It is worth mentioning that the pre-cooling load serves as an accessibility option for BTMS. When it encounters with extreme ambient temperatures or severe operation conditions such as super fast charging and high-speed cruising, this feature is activated to provide a stronger cooling capability towards thermal control via cooling down the approaching air. In general, the control-oriented dynamic temperature response of the vehicle cabinet can be formulated as follows:

$$T_{in(k+1)} = T_{in(k)} + \frac{(Q_{cr}+Q_{cw}+Q_r+Q_h+Q_f+Q_s+Q_b)-Q_{ac}}{\rho_{air}V_{in}C_{air}}\delta t \tag{10}$$

where the cabinet volume V_{in} equals to 3 m^3, and δt denotes the time-step in seconds. Note that the hysteresis effects from both the power train and the liquid-loop are not considered here. The adjustment of cabin air temperature is controlled by adjusting the total power input for the AC system with basic control logistics. Detailed modeling and controlling of the air conditioning system, including the compressor, the fan, and the condenser, are beyond the research scope of this paper.

2.5 BTMS Energy Consumption Model. In the concept design of the *J*-type BTMS, the cooling air is actuated by an air fan under normal conditions. When the ambient temperature is higher than the predefined threshold or encountering severe operating conditions, a heat exchanger will be activated to pre-cool the air, in which the coolant comes directly from the AC system, as shown

Table 2 Vehicle cabin thermal modeling

Physical term	Symbol	Heat source	Temperature	Estimation (W)	Descriptions and highlights
Conduction/ convection load via roof panel	Q_{cr}	External air solar radiation	Dependent	Eq. 9 or without radiation $Q_{cr}=k_{cr}A(T_{ex}-T_{in})$ $k_{cr}=(\sum\frac{\delta}{\lambda}+\frac{1}{h_{in}}+\frac{1}{h_{ex}})^{-1}$	δ: thickness; λ:conductivity; $A=3.6\,m^2$; $h_{in}=25\,W/(m^2K)$; $h_{ex}=4.65+13.96\sqrt{v}$
Conduction/ convection load via windows	Q_{cw}	External air solar radiation	Dependent	Eq. 9 or without radiation $Q_{cw}=\sum k_{cw}A(T_{ex}-T_{in})$ $k_{cw}=(\frac{\delta}{\lambda}+\frac{1}{h_{in}}+\frac{1}{h_{ex}})^{-1}$	$A=1.5\,m^2$; $h_{in}=25\,W/(m^2K)$; $h_{ex}=4.65+13.96\sqrt{v}$
Solar radiation through windows	Q_r	Solar flux	Independent	$Q_r=\sum_{i=1}^{n=4}\eta IA_i sin\theta_i\beta$	Four windows: windshield, rear, left, right; β: shading factor; θ: installation angle; η: penetration rate; I: incident radiation
Human body thermal load	Q_h	Driver& Passenger(s)	Independent	$Q_h=145+116n$ [40]	n: passengers number; n=3
Fresh air thermal load	Q_f	Fresh air	Dependent	$Q_f=\xi\dot{m}_{air}C_{air}(T_{ex}-T_{in})$	Ventilation fresh air portion $\xi=12\%$; $\dot{m}_{air}=0.186$ kg/s
Sensible heat load	Q_s	Cabin interior	Dependent	$Q_s=h_c\,A_c\,(T_c-T_{in})\;T_c(k+1)=T_c(k)-Q_s/(C_cm_c)$	$h_c=20\,W/(m^2K)$; $A_c=8\,m^2$; $m_c=200\,kg$; $C_c=1500\,J/(kgK)$
BTMS pre-cooling load	Q_b	Pre-cool BTMS	Dependent	$Q_b=\dot{m}C_{air}(T_{ex}-T_{air})$	$\dot{m}$: BTMS cooling air flowrate T_{air}: pre-cooled temperature

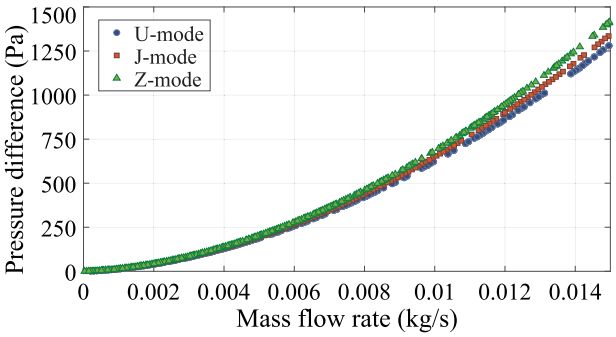

Fig. 5 The relationship between the pressure augment and the mass flowrate for *U*-, *J*-, and *Z*-type structures

in Fig. 1. The fan power is estimated by

$$P_{btms} = \frac{\dot{m} P_c}{\rho \eta_c} \tag{11}$$

where P_c is the pressure augment of the compressor, ρ is the air density, and η_c is the flow efficiency. All the properties and parameters are obtained via CFD simulations, and the relationship is approximated using a support vector regression model, as shown in Fig. 5.

Besides the aforementioned systems, other major subsystems and devices include the power steering, the braking system, the lights, and the entertainments. Due to the complexities under dynamic conditions, it is challenging to establish a comprehensive dynamic model that consists of all these subsystems. In this paper, as a trade-off, only the driving motor with regenerative function, the air conditioner, and the thermal control system are considered and modeled in detail, while other auxiliary devices are assigned with an estimated fluctuated power that follows a normal distribution as follows.

$$P_{aux} \sim \mathcal{N}(\mu, \alpha^2) = \mathcal{N}(1000, 250) \tag{12}$$

3 The Thermal Control Framework and Energy Management Strategy

3.1 The Control System of BTMS. A neural network (NN)-based battery thermal control system has been developed in our previous study [22], which consists of a temperature prediction model, an NN-aided controller that is integrated with MPC, and a mode switching module, as shown in Fig. 6. The feasibility and effectiveness of the control system as well as the control strategy have been validated in Ref. [7]. Note that the conceptual framework neglects the bias in measurement as well as the bias between the simulated plant and its corresponding real battery system.

Based on the results from transient CFD simulations, a multi-input multi-output (MIMO) battery temperature prediction model

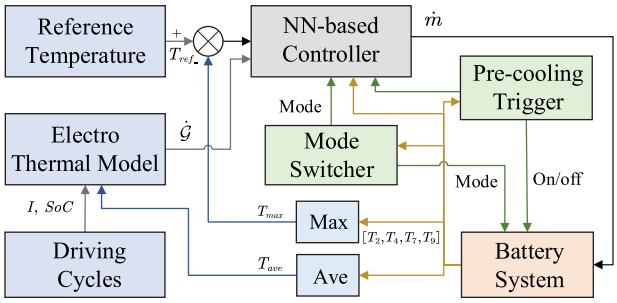

Fig. 6 The control framework of the air-based *J*-type BTMS

is implemented with a neural network algorithm, under conditions with two different approaching air temperatures for *J*-, *U*-, and *Z*-mode, given as

$$[T_2, T_4, T_7, T_9]_{k+1} = \mathcal{F}(T_{ave}, T_{air}, \dot{m}, \dot{\mathcal{G}}) + [T_2, T_4, T_7, T_9]_k \tag{13}$$

where the operation temperature T_{ave} is defined as the average of the four monitoring temperatures. The cooling air temperature T_{air} is set as 300 K under normal conditions, whereas the air temperature is pre-cooled to 293 K with the cabin AC system.

The NN-aided controller aims to generate a reasonable mass flowrate considering the temperature bias between the battery pack and the reference trajectory, the operation temperature, the air temperature, the heat generation rate, and the systematic operation mode, expressed as

$$\begin{aligned} \dot{m} &= \mathcal{C}(T_{bias}, T_{ave}, T_{air}, \dot{\mathcal{G}}) \\ T_{bias} &= T_{ref} - \max(T_2, T_4, T_7, T_9) \end{aligned} \tag{14}$$

As regards the mode switching module, the switching temperature criterion is defined as the temperature difference between the left side and right side.

$$T_{sw} = \max(T_2, T_4) - \max(T_7, T_9) \tag{15}$$

The critical criteria of switching to *U*-, *Z*-, and *J*-mode are defined as $\mathcal{S}_u$:$T_{sw} \geq 0.5$ K, $\mathcal{S}_z$:$T_{sw} \leq -0.5$ K, and $\mathcal{S}_j$:$|T_{sw}| \leq 0.2$ K, respectively. Note that the mode switching is requested to follow switching sequences like [*J*-*U*-*Z*-1/2*U*-*J*] and [*J*-*Z*-*U*-1/2*Z*-*J*] to complete an entire switching cycle, in which the system traverses a complete *J*-, *U*-, *Z*-mode, and a half stroke of either *U*- or *Z*-mode in sequence before it cycles back to *J*-mode. Due to the actuator's operation limitations, the first constraint limits the operation range, while the second constraint confines the changing rate, as expressed by

$$\begin{aligned} 0 \leq \dot{m} \leq 0.012 \\ |\Delta \dot{m}| \leq 0.003 \end{aligned} \tag{16}$$

3.2 The Control System of Air Conditioning System. Based on the cabin thermal load model developed in Sec. 2.4, a control-oriented AC thermal system can be established. The cabin temperature is selected as the system output and the AC cooling capability is chosen as the control variable, as formulated by

$$\begin{cases} \dot{x} = \dfrac{(Q_{cr} + Q_{cw} + Q_r + Q_h + Q_f + Q_s + Q_b) - u}{\rho_{air} V_{in} C_{air}} \\ y = x \end{cases} \tag{17}$$

where both x and y denote the cabin temperature T_{in}, and u represents the cooling capacity Q_{ac}. A basic proportional-integral (PI) controller is developed to control the temperature of the cabin temperature with a targeted value of 294 K. Parameters of the PI controller are tuned based on the situation without the pre-cooling function. For the sake of energy efficiency, limitations other than the targeted value are not imposed on the thermal control.

It is worth mentioning that the pre-cooling thermal load for BTMS, Q_b, only activates at a certain time, and the cabin climate control may probably be affected, since the cooling capacity of the AC system is limited and the BTMS has a higher priority over the cabin thermal management. When the maximum temperature of the battery pack exceeds 311.8 K, the pre-cooling function is activated, whereas it is deactivated after the temperature declines back to 310 K. The constraints are formulated based on the limitations proposed in Ref. [40], including an operation boundary and a changing rate limitation as follows:

$$\begin{aligned} 0 \leq Q_{ac} \leq 4500 \eta_{cop} \\ |\Delta Q_{ac}| \leq 1000 \end{aligned} \tag{18}$$

3.3 Energy Management Strategy. The energy management strategy aims to enhance the energy efficiency as well as the battery health performance via an MPC algorithm, while retaining the constraints from the perspectives of thermal limitations and electrical requirements. The considerations and approaches are predefined in a twofold manner: (i) to avoid potential overlapping peaks by rescheduling the operation of different devices; (ii) to mitigate the negative effects regarding the battery cycle-life in recharging the battery by distributing the regenerative energy to auxiliary systems. By adopting an MPC algorithm, the thermal control and centralized optimization framework is formulated as follows:

$$\begin{aligned} \underset{Q_{ac},\dot{m}}{\text{argmin}}\ J = & \sum_{k=n}^{n+N} (\alpha_k (P_{drv_k} + P_{aux_k} + P_{ac_k} + P_{bs_k})^2 \\ & + \beta_k (T_{re\,f_k} - T_{b_k})^2 + \xi_k (T_{tar_k} - T_{in_k})^2) \\ \text{subject to}\quad & 0 \le \dot{m} \le 0.012 \\ & |\Delta \dot{m}| \le 0.003 \\ & 0 \le Q_{ac} \le 4500 \eta_{cop} \\ & |\Delta Q_{ac}| \le 1000 \end{aligned} \tag{19}$$

where n is the current step and N is the control horizon. Based on specific control purposes, penalty coefficients α_k, β_k, and ξ_k are preset to attribute weights of the overall power consumption, the control target temperatures of the cabin and the battery, respectively. The soft constraints of the two subsystems are implemented via a real-time adjustment of the corresponding coefficient, i.e., the temperature biases should be constrained within 0.5 K and 1 K for BTMS and AC, respectively. Since the second term about the thermal control of the battery system involves safety concerns, a larger weighting, β_k, is assigned to BTMS compared with the AC system.

A particle swarm optimization (PSO) algorithm is employed to solve the problem, in which PSO starts with the original direct control solutions of the two subsystem. It is worth mentioning that the stochastic PSO approach is promising to obtain a reasonable solution instead of a global optimum within limited calculation time by tuning different convergence criteria.

4 Results and Discussion

An integrated driving cycle that consists of the EPA urban dynamometer driving schedule (UDDS), the world-harmonized light-duty vehicles test cycle (WLTC), and the highway fuel economy driving schedule (HWFET) is directly utilized to test and validate the energy management strategy [42]. Combined with the power consumption from auxiliary devices, the uncontrollable power consumptions, i.e., as the management system inputs, are presented in Fig. 7. The sample time is set to be 5 s.

4.1 No Energy Management Strategy. The BTMS and AC systems are operated separately based on their own conditions without a global energy management strategy. For BTMS, the power consumption of the last step is taken into consideration to calculate the heat generation rate for the current step, and thus determine the mass flowrate, as shown in Fig. 8. The temperature distribution of the battery pack along the dynamic process is presented in Fig. 9. It is seen that the temperatures follow close behind the targeted reference trajectory via switching among the *J*-, *U*-, and *Z*-mode. Due to the flow characteristic of *Z*-mode, the battery cells near the right outlets have a stronger heat dissipation capability under large flowrate conditions. The temperature uniformity deteriorates after 2,100 s, while the maximum temperature in the ninth battery cell also decreases. At around 2,950 s, the pre-cooling module activates to provide extra cooling capacity to cope with the large amount of heat generation. Overall, the BTMS is capable to retain the temperature within an expected range.

For the AC, though the temperature of the internal air goes down in a fast manner, the base temperature decreases very slowly because of limited convection heat transfer, as shown in Fig. 10. The velocity variations may inevitably bring about fluctuations to the cabin temperature as well as the power usage. Only a base load is required to balance the sensible heat from solar radiation and the human body under normal operations.

4.2 Model Predictive Control-Based Energy Management Strategy. Based on the MPC algorithm developed in Sec. 3.3, the forecast horizon is set to be five steps or 25 s. Aiming to reduce the overall power usages, the power consumptions of BTMS and AC are scheduled flexibly according to the real-time driving and auxiliary power usage. Both the BTMS and AC have similar and accepted performances compared with that of no energy management, as presented in Figs. 11 and 12. However, it is observed that the power consumption of BTMS is reduced for the reason that the overall heat generation is reduced by lowering the peak load, which is implemented by shifting the operation with AC, as shown in Fig. 13. For instance, the operation of AC

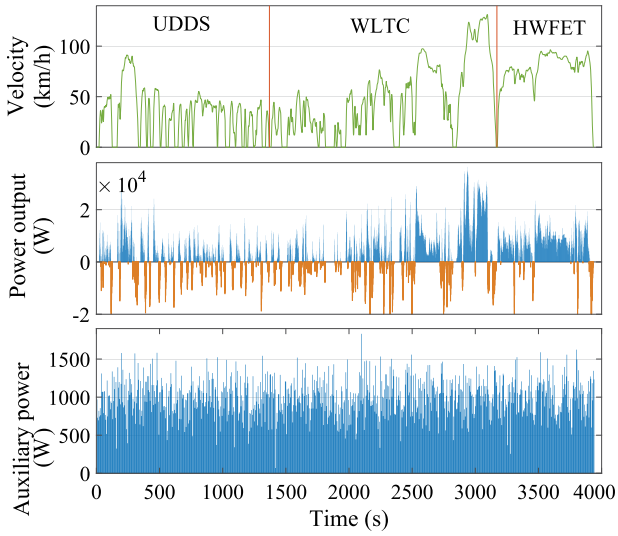

Fig. 7 The power consumptions of tested driving cycles and auxiliary devices

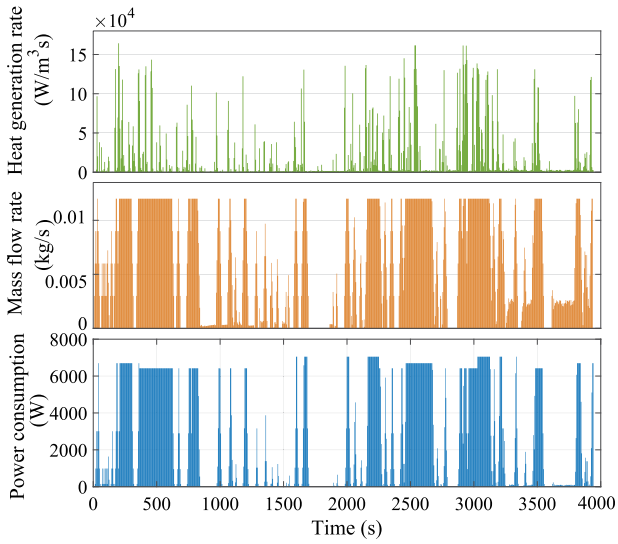

Fig. 8 The BTMS properties without energy management

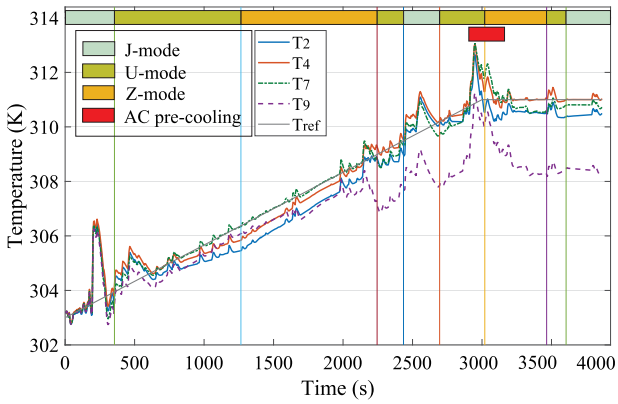

Fig. 9 The BTMS temperature distribution without energy management

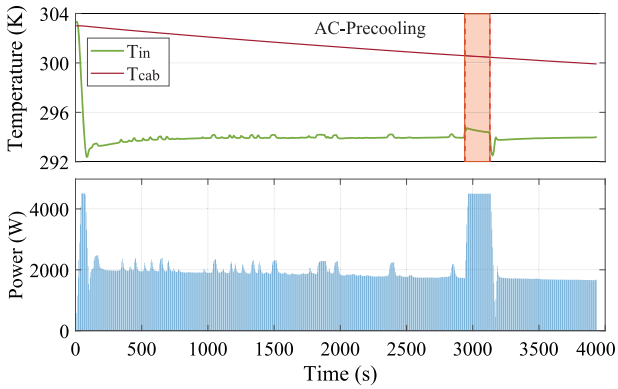

Fig. 10 The AC performance without energy management

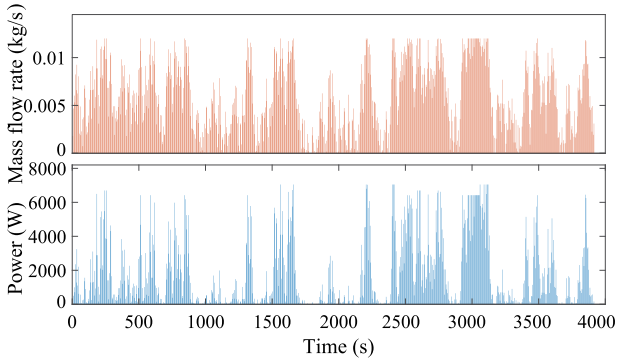

Fig. 11 The BTMS properties with MPC-based energy management

almost completely terminates at around 200–300 s and 2600–2650 s to avoid overlapping with existing load peaks.

It is also seen that the regeneration power that recharges back to the battery system is reduced by 4.3% from 8809 J to 8430 J per battery cell, at the cost of bringing about extra fluctuations in the temperature controls of BTMS and AC system. The total energy consumption also has a 6.5% improvement from MPC with a value of 23,800 J compared with 25,500 J without any management strategy per battery. Moreover, the final stage SoC with MPC is 0.5864 compared to 0.5653 for the system without control, which has a 3.8% improvement. Note that the developed algorithm and control framework are also applicable to liquid-based battery cooling system, since they share similarities in terms of fluidity and controllability.

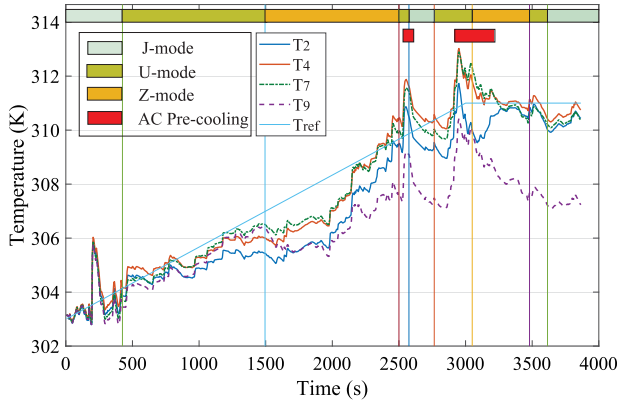

Fig. 12 The battery temperature distribution with MPC-based energy management

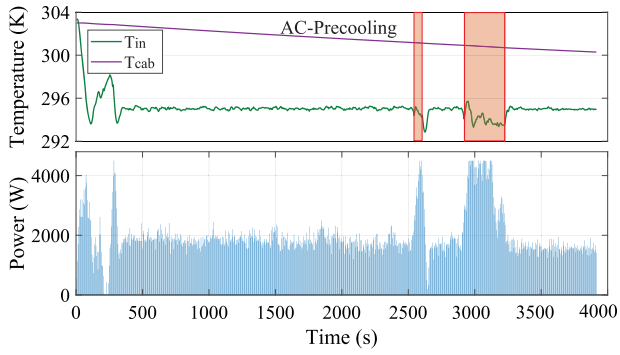

Fig. 13 The A performance with MPC-based energy management

5 Conclusion

This paper developed an MPC-based energy management strategy to control the electric vehicle cabin climate system and battery thermal management system simultaneously. A battery thermal control model was developed using neural network, while the cabin air conditioning system was established with a proportional-integral control method. The energy management strategy aims to reduce the values of load peaks, while retaining the constraints of the BTMS and AC systems.

The MPC-based energy management strategy was tested using an integrated driving cycle. Compared to the system with no energy management, no significant differences were observed in terms of thermal properties and dynamic balance. However, from the perspective of energy efficiency, simulation results revealed that there were a 4.3% reduction for the recharging energy, and a 6.5% improvement for the overall energy consumption. It is shown that the MPC-based energy management is a promising solution to enhance the overall efficiency of EVs.

Potential future work will seek to reduce the computational complexity by linearizing the system or employing decentralized MPC approaches. Moreover, we also attempt to adopt a hierarchical multi-system vertical model predictive control algorithm to strengthen the control for the battery thermal management system and cabin AC system.

References

[1] Liu, H., Wei, Z., He, W., and Zhao, J., 2017, "Thermal Issues About Li-Ion Batteries and Recent Progress in Battery Thermal Management Systems: A Review," Energy Convers. Manage., **150**, pp. 304–330.

[2] Lu, L., Han, X., Li, J., Hua, J., and Ouyang, M., 2013, "A Review on the Key Issues for Lithium-Ion Battery Management in Electric Vehicles," J. Power. Sources., **226**, pp. 272–288.

[3] Akinlabi, A. H., and Solyali, D., 2020, "Configuration, Design, and Optimization of Air-cooled Battery Thermal Management System for Electric Vehicles: A Review," Renewable. Sustainable. Energy Rev., **125**, p. 109815.
[4] Wang, X., Li, M., Liu, Y., Sun, W., Song, X., and Zhang, J., 2017, "Surrogate Based Multidisciplinary Design Optimization of Lithium-Ion Battery Thermal Management System in Electric Vehicles," Struct. Multidiscipl. Optim., **56**(6), pp. 1555–1570.
[5] Wang, X., Liu, Y., Sun, W., Song, X., and Zhang, J., 2018, "Multidisciplinary and Multifidelity Design Optimization of Electric Vehicle Battery Thermal Management System," ASME J. Mech. Des., **140**(9), p. 094501.
[6] Dandurand, B., Guarneri, P., Fadel, G., and Wiecek, M. M., 2013, "Equitable Multi-Objective Optimization Applied to the Design of a Hybrid Electric Vehicle Battery," ASME J. Mech. Des., **135**(4), p. 041004.
[7] Liu, Y., and Zhang, J., 2019, "Design a J-Type Air-Based Battery Thermal Management System Through Surrogate-Based Optimization," Appl. Energy, **252**, p. 113426.
[8] Wang, S., Li, K., Tian, Y., Wang, J., Wu, Y., and Ji, S., 2019, "Improved Thermal Performance of a Large Laminated Lithium-Ion Power Battery by Reciprocating Air Flow," Appl. Therm. Eng., **152**, pp. 445–454.
[9] Xun, J., Liu, R., and Jiao, K., 2013, "Numerical and Analytical Modeling of Lithium Ion Battery Thermal Behaviors With Different Cooling Designs," J. Power. Sources., **233**, pp. 47–61.
[10] Yu, X., Lu, Z., Zhang, L., Wei, L., Cui, X., and Jin, L., 2019, "Experimental Study on Transient Thermal Characteristics of Stagger-Arranged LithiumI-on Battery Pack With Air Cooling Strategy," Int. J. Heat. Mass. Transfer., **143**, p. 118576.
[11] Wang, T., Tseng, K., Zhao, J., and Wei, Z., 2014, "Thermal Investigation of Lithium-Ion Battery Module With Different Cell Arrangement Structures and Forced Air-Cooling Strategies," Appl. Energy, **134**, pp. 229–238.
[12] Gao, X., Ma, Y., and Chen, H., 2018, "Active Thermal Control of a Battery Pack Under Elevated Temperatures," IFAC-PapersOnLine, **51**(31), pp. 262–267.
[13] He, F., and Ma, L., 2015, "Thermal Management of Batteries Employing Active Temperature Control and Reciprocating Cooling Flow," Int. J. Heat. Mass. Transfer., **83**, pp. 164–172.
[14] Wang, H., He, F., and Ma, L., 2016, "Experimental and Modeling Study of Controller-based Thermal Management of Battery Modules Under Dynamic Loads," Int. J. Heat. Mass. Transfer., **103**, pp. 154–164.
[15] Masoudi, Y., Mozaffari, A., and Azad, N. L., 2016, "Battery Thermal Management of Electric Vehicles: An Optimal Control Approach," ASME 2015 Dynamic Systems and Control Conference, Columbus, OH, American Society of Mechanical Engineers Digital Collection.
[16] Tao, X., and Wagner, J., 2016, "A Thermal Management System for the Battery Pack of a Hybrid Electric Vehicle: Modeling and Control," Proc. Inst. Mech. Eng., Part D: J. Aut. Eng., **230**(2), pp. 190–201.
[17] Masoudi, Y., and Azad, N. L., 20172017, "Mpc-Based Battery Thermal Management Controller for Plug-in Hybrid Electric Vehicles," American Control Conference (ACC), Seattle, WA, IEEE, pp. 4365–4370.
[18] Amini, M. R., Wang, H., Gong, X., Liao-McPherson, D., Kolmanovsky, I., and Sun, J., 2019, "Cabin and Battery Thermal Management of Connected and Automated Hevs for Improved Energy Efficiency Using Hierarchical Model Predictive Control," IEEE Trans. Control Syst. Tech., **28**(5), pp. 1711–1726.
[19] Guanetti, J., Kim, Y., and Borrelli, F., 2018, "Control of Connected and Automated Vehicles: State of the Art and Future Challenges," Annual Rev. Control, **45**, pp. 18–40.
[20] Amini, M. R., Sun, J., and Kolmanovsky, I., 20182018, "Two-layer Model Predictive Battery Thermal and Energy Management Optimization for Connected and Automated Electric Vehicles," IEEE Conference on Decision and Control (CDC), Miami, FL, IEEE, pp. 6976–6981.
[21] Yang, Z., Li, K., and Foley, A., 2015, "Computational Scheduling Methods for Integrating Plug-in Electric Vehicles With Power Systems: A Review," Renewable Sustainable Energy Rev, **51**, pp. 396–416.
[22] Liu, Y., and Zhang, J., 2019, "Self-Adapting Intelligent Battery Thermal Management System Via Artificial Neural Network Based Model Predictive Control," ASME 2019 International Design Engineering Technical Conferences and Computers and Information in Engineering Conference, Anaheim, CA.
[23] Zhang, X., Kong, X., Li, G., and Li, J., 2014, "Thermodynamic Assessment of Active Cooling/heating Methods for Lithium-Ion Batteries of Electric Vehicles in Extreme Conditions," Energy, **64**, pp. 1092–1101.
[24] Peters, D. L., Papalambros, P. Y., and Ulsoy, A. G., 2013, "Sequential Co-Design of An Artifact and Its Controller Via Control Proxy Functions," Mechatronics, **23**(4), pp. 409–418.
[25] Allison, J. T., Guo, T., and Han, Z., 2014, "Co-design of An Active Suspension Using Simultaneous Dynamic Optimization," ASME J. Mech. Des., **136**(8), p. 081003.
[26] Herber, D. R., and Allison, J. T., 2019, "Nested and Simultaneous Solution Strategies for General Combined Plant and Control Design Problems," ASME J. Mech. Des., **141**(1), p. 011402.
[27] Song, Z., Hofmann, H., Li, J., Han, X., Zhang, X., and Ouyang, M., 2015, "A Comparison Study of Different Semi-active Hybrid Energy Storage System Topologies for Electric Vehicles," J. Power. Sources., **274**, pp. 400–411.
[28] Yang, Z., Patil, D., and Fahimi, B., 2018, "Online Estimation of Capacity Fade and Power Fade of Lithium-ion Batteries Based on Input–output Response Technique," IEEE Trans. Trans. Electrification, **4**(1), pp. 147–156.
[29] Yang, Z., Patil, D., and Fahimi, B., 2019, "Electrothermal Modeling of Lithium-ion Batteries for Electric Vehicles," IEEE Trans. Vehicular Tech., **68**(1), pp. 170–179.
[30] Liu, Y., and Zhang, J., 2020, "Self-Adapting J-type Air-Based Battery Thermal Management System Via Model Predictive Control," Appl. Energy, **263**, p. 114640.
[31] Liu, Y., Ghassemi, P., Chowdhury, S., and Zhang, J., 2018, "Surrogate Based Multi-objective Optimization of J-type Battery Thermal Management System," ASME 2018 International Design Engineering Technical Conferences and Computers and Information in Engineering Conference, Quebec, Canada.
[32] Evtimov, I., Ivanov, R., and Sapundjiev, M., 2017, "Energy Consumption of Auxiliary Systems of Electric Cars," MATEC Web of Conferences, EDP Sciences, Sozopol, Bulgaria., Vol. 133, p. 06002.
[33] Chandak, G. A., and Bhole, A., 20172017, "A Review on Regenerative Braking in Electric Vehicle," Innovations in Power and Advanced Computing Technologies (i-PACT), Vellore, India, IEEE, pp. 1–5.
[34] Tesla. "Tesla model 3 specification." Available at https://www.tesla.com/model3.
[35] Laboratory, I. N. "Ev auxiliary systems impacts." Available at https://avt.inl.gov/sites/default/files/pdf/fsev/auxiliary.pdf
[36] Qi, Z., 2014, "Advances on Air Conditioning and Heat Pump System in Electric Vehicles–a Review," Renewable Sustainable Energy Rev., **38**, pp. 754–764.
[37] Khayyam, H., Kouzani, A. Z., Hu, E. J., and Nahavandi, S., 2011, "Coordinated Energy Management of Vehicle Air Conditioning System," Appl. Therm. Eng., **31**(5), pp. 750–764.
[38] Pino, F. J., Marcos, D., Bordons, C., and Rosa, F., 2015, "Car Air-conditioning Considerations on Hydrogen Consumption in Fuel Cell and Driving Limitations," Int. J. Hydrogen Energy, **40**(35), pp. 11696–11703.
[39] Marcos, D., Pino, F. J., Bordons, C., and Guerra, J. J., 2014, "The Development and Validation of a Thermal Model for the Cabin of a Vehicle," Appl. Therm. Eng., **66**(1–2), pp. 646–656.
[40] He, H., Jia, H., Sun, C., and Sun, F., 2018, "Stochastic Model Predictive Control of Air Conditioning System for Electric Vehicles: Sensitivity Study, Comparison, and Improvement," IEEE Trans. Indus. Inform., **14**(9), pp. 4179–4189.
[41] Kiss, T., Chaney, L., and Meyer, J., 2013, "New automotive air conditioning system simulation tool developed in matlab/simulink." Technical Report, National Renewable Energy Lab. (NREL), Golden, CO.
[42] Geller, B. M., and Bradley, T. H., 2015, "Analyzing Drive Cycles for Hybrid Electric Vehicle Simulation and Optimization," ASME J. Mech. Des., **137**(4), p. 041401.